Institute of Space and Aeronautical Science University of Tokyo
Report No. 393, January 1965

Diffraction of a Plane Shock Wave Around a Corner

By

Koichi OSHIMA, Katsutaka SUGAYA, Masao YAMAMOTO,
and Toshio TOTOKI

Summary. Diffraction of a plane shock wave around a sharp convex 90° corner was observed in a shock tube flow with the various shock Mach numbers from 2.8 to 1.5. The shock wave shape observed showed quantitative difference from the theoretical predictions, which are derived from the one-dimensional flow theory and the ray-shock theory. Considering the possible cause of this discrepancy, it is suggested, the shear stress due to turbulent-like mixing between the ray tubes immediately behind the shock front may play an important role in this phehomenon. On the basis of the concept of the turbulent mixing length, a generalized theory, which includes this shear effect, is proposed and a linearized solution of this equation is obtained. The predicted results show good agreement with the experimental data.

1. INTRODUCTION

As shown in Fig. 1, let us consider a plane shock wave with a finite strength, which propagates along a plane wall and diffracts around a sharp convex corner at a certain angle, say $\pi/2$ radian. Of course, the flow pattern in such case can be calculated by a step-by-step numerical method solving the unsteady two-dimensional gasdynamic equations with an indeterminate boundary, i.e. a shock wave [*1*], if a good computor could be available, but the true physical meanings of the phenomenon are often lost under a heavy pile of the numerical data. Here we will discuss about analytical approximations of this kind of problems based on experimental data observed in a shock tube flow. The physical importance of such studies has been well emphasized, for example, in a recent paper by D. C. Pack [*2*]. Unfortunately some definite discrepancies between the analytical predictions basing on the existing theories and the experimental data, not only on the diffracted shock wave shape but also on the observed flow patterns behind the shock wave, were found. Thus, it is one of the purposes of this paper to discuss all the possible causes of this failure of these theories. All the evidences found strongly suggest that the momentum transfer through the transverse direction to the flow due to shear stress may play an important role in this phenomenon.

Following Whitham's papers [*3*] and [*4*], we introduce a set of curves formed by the successive positions of curved shock as it moves forward through a uniform medium, which will be called 'shock fronts' or simply 'shocks', and another set of curves of the orthogonal trajectories of these shock fronts, which will be called 'rays'. In Fig. 1 the positions of shocks are shown by full lines and the rays are shown by broken lines on a physical plane with the Cartesian coordinates (X, Y).

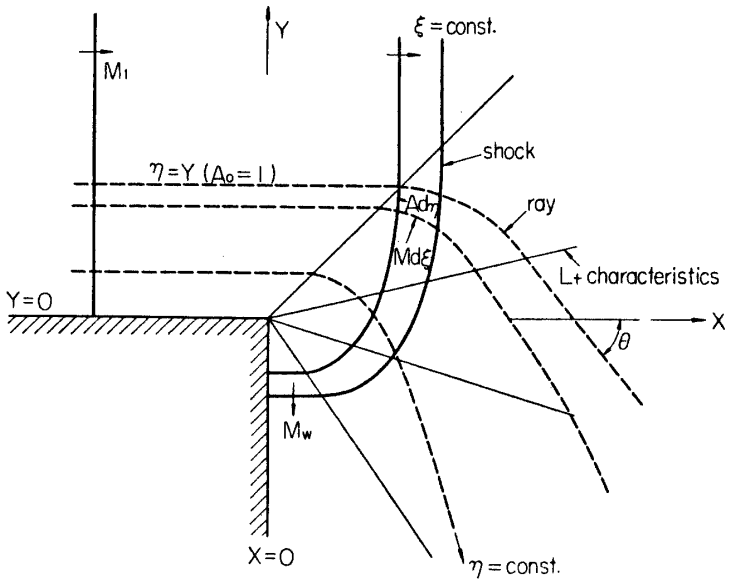

FIGURE 1. Diffraction of a plane shock wave around a corner.

The shape of the wall is also shown in the figure. Coordinates (ξ, η) are introduced such that the shock positions are the curves $\xi=$constant, and the rays are $\eta=$constant. As ξ abscissa takes $\xi=a_0 t$ where a_0 is the sound speed in the uniform gas ahead of the shock. Then, the distance along a ray between the shock positions given by ξ and $\xi+d\xi$ is $Md\xi$ where M is the Mach number of the shock at a point (ξ, η). If we let $Ad\eta$ be the corresponding distance between the rays η and $\eta+d\eta$, then it can be seen that, for purely geometrical reasons, M and A must satisfy the differential equations

$$\begin{aligned} \frac{\partial \theta}{\partial \eta} &= \frac{1}{M}\frac{\partial A}{\partial \xi} \\ \frac{\partial \theta}{\partial \xi} &= -\frac{1}{A}\frac{\partial M}{\partial \eta}, \end{aligned} \tag{1.1}$$

where θ is the angle made by the ray with the initial direction of the shock propagation. This relation was derived by Whitham [3]. Now if M depends only upon A, and vice versa, and if we could find an explicit relation between them, the shock positions can be determined for all times, since the equations (1.1) are a system of homogeneous quasi-linear partial differential equations with the two dependent variables θ and $A(M)$ and the two independent variables (ξ, η) provided with $dA/dM<0$. This kind of analysis, which was originally presented by Whitham, will be called the ray-shock theory and its detailed discussions will appear in the chapter 4, and an improved form of it in the chapter 6.

This $A-M$ relation requires a strict solution of the equations of motion for the flow behind the shock, subject to the Rankine-Hugoniot relations across the shock and the boundary conditions at solid walls, etc. Naturally, this implies the failure of our first assumption, that is, M depends not only upon A but also upon the flow field behind the shock front. However, the above approach suggests a

simple approximate procedure, in which we assume that the propagation of the shock between any two neighbouring rays can be treated as if the rays have solid walls. This would be exactly true, if the rays were particle paths, but what we can say at most is that immediately behind the shock the particles move normal to the shock, i.e. in the ray direction. However, we assume that the later divergence of the rays and the particle paths is not important, which will be justified by later discussions, and accept this similarity to propagation in a channel. Thus, from the analysis of the one-dimensional channel flow, we may find a functional relation

$$A=A(M)\,. \tag{1.2}$$

This is given as a solution of the gasdynamic equations of unsteady one-dimensional flow with varying cross section provided with the known ray tube geometry. Of course, these are given as the solution of the original problem.

In the chapter 2, in order to obtain this $A-M$ relation, we consider a shock moving down a channel which initially has a constant cross section and then downstream part with varying cross section, as shown in Fig. 2. If the modifications to the shock arise only from changes in channel areas, we can derive the

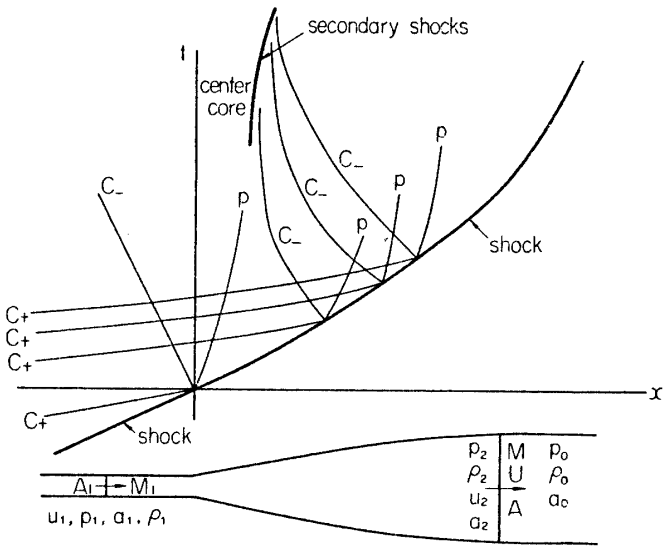

FIGURE 2. Schematic $x-t$ diagram in the characteristic rule.

functional dependence between A and M. This relation was given by Chester [5], used by Chisnell [6] and later re-derived on the broader bases by Whitham [7], but little is known about the accuracy of this relation. For some problems this relation gives the reasonable results comparing with the numerical calculations as well as the experimental results. Yet, the true reason why this approximation gives so good results has been, as Whitham said, open to question. This rule is usually called the characteristic rule. Several years later, Rościszewski discussed the characteristic equations and gave the wider applications of this idea [8]. In this paper, in order to check the accuracy of this rule, we derive this relation on

a more exact mathematical argument and determine the forms of the missing terms, mainly following the Rościszewski's analysis. This rule is obtained in such a way that a characteristic form of the basic equations is integrated along the corresponding characteristic line from the initial uniform flow portion until the shock front and differentiated with respect to the tube distance. In the resulting equation, the terms which are not derived from the conditions at the shock front can be omitted, if the influence of the other families of characteristics does not exist. In this point of view, this treatment shows a close relationship with the simple wave theory of the homogeneous hyperbolic equations. In this report, these neglected terms are evaluated using the linearized solution [6] and [9], which gives the second order terms of the characteristic rule. The result assures the usefulness of this rule, moreover the linearized theory can prescribe the flow field behind the shock front, especially, it predicts the existence of the secondary shock wave at a position where a strong variation of the flow field is experimentally observed.

As seen from this analysis, this characteristic rule cannot give a proper prediction in such cases where the area change is very large or some time after the secondary shock is formed. Furthermore, these corrections are found to be quite insufficient to explain the observed discrepancies between theory and experiments.

On the other hand, we have various blast wave theories, which might be useful for the cases with a large expansion ratio of the cross section or the flow field far from the complicated center region [10]. For weak blast waves, which correspond to our experiments, the weak blast wave theory is most suitable [11], in which the motion of the shock front is determined by two characteristics; one is on-coming C_+ characteristics whose characters are determined by the local upstream flow features and the other is out-going C_- characteristics whose characters depend on the shock front condition started, as shown in Fig. 3. This weak blast wave theory will be discussed in the chapter 3, together with the geometrical acoustic

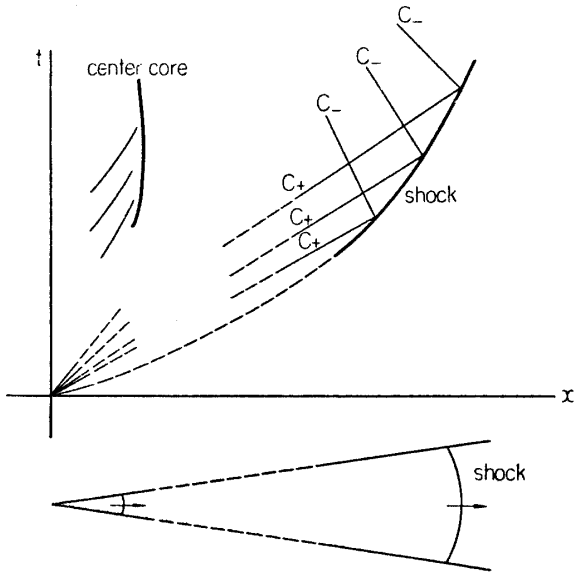

FIGURE 3. Schematic $x-t$ diagram in the weak blast wave theory.

theory, which corresponds to the lower order approximation of the weak blast wave theory. In general, the blast wave is an outward propagating shock wave caused by an instantaneously released energy on a point (for a spherical blast wave) or on a line (for a cylindrical blast wave) or on a plane (for a planer blast wave). Its feature is, it is confirmed both experimentally and theoretically [10], well prescribed by Taylor's self-similar theory and Sakarai's second order theory for the strong blast waves and the quasi-similarity theory for the moderately strong blast waves. In these blast wave analyses, it is considered that the explosion takes place at $t=0$ and at a point (or on a line or on a plane) $x=0$, therefore all the characteristics start at $t=0$, $x=0$, and they are reflected by the blast wave front and interact with the on-coming characteristics. After the elapse of some time, these backward-going characteristics concentrate around the center and create some complicated patterns, i.e. the secondary shock waves or the center core, but the characteristics starting from this center part can hardly reach the front part of the blast wave, where flow features, then, are determined almost solely by the on-coming characteristics starting at the initial moment and the first reflected characteristics by the blast wave front. This means that the blast wave flow is determined by the C_+ characteristics and the first C_- characteristics and reveals the definite constrast to the channel flow treated before, in which the C_+ characteristics start continuously at $x<0$ under the constant condition and the effect of the C_- characteristics is neglected. This is the reason why the decay coefficient for the blast wave could be applied to the shock wave diffracted around a sharp corner at a large angle, especially if the flow behind the diffracted shock wave has a complicated feature. The solution is obtained by expanding the flow quantities in the power series of the approximated characteristic line. The zeroth order term is the well-known geometrical acoustics and the first order terms correspond to the weak shock theory. Assuming a proper ray-tube geometry, we have an $A-M$ relation, which is used to solve the equation (1.1). However, the $A-M$ relation obtained gives even larger discrepancies between the theory and the experiments than those by the characteristic rule.

The results obtained by these two methods give the weaker diffracted shock wave than those experimentally observed. Various correction terms and various ray tube geometries are insufficient to explain this discrepancy. All the possible corrections or modifications on the $A-M$ relations based on the one-dimensional flow analysis are proved to be unable to give such low rate of attenuation of the shock wave propagating through an expanding tube that the experimental data request. Therefore this low rate of attenuation of the diffracted wave should be caused by another reason, which may come from some interactions between the neighbouring tubes following the shock fronts with different strengths. The detailed mechanism of this mixing process between the neighbouring ray tubes has not been clear, but we assume the somewhat similar process as the turbulent mixing which is usually observed in the incompressible fully developed turbulent jet or channel flow, though any turbulent like character, in the usual sence, is not observed within the flow field in consideration. Here it is worthwhile to note that the ray-

tube theory fails to give a meaningful solution for cases with large diffraction angle of a relatively weak shock wave and that the reason for this failure is explained due to the flow separation around the corner. However the diffracted shock wave is experimentally observable for all the cases where the ray-shock theory cannot give a solution, and the observed flow pattern shows a strong vortex-like density variation in the neighbourhood of the corner. Therefore it might be acceptable to assume that the large scale mixing actually takes place and to adopt the mixing length hypothesis [*15*] in order to obtain a rough estimation of this phenomenon. In the chapter 5, starting with the unsteady one-dimensional gas-dynamic equations including a term of mixing with the neighbouring flow, we derive a generalized characteristic rule.

In the chapter 6, using this rule, the ray-shock theory is generalized, which necessarily contains higher order derivatives due to this effect. A linearization of this generalized equation for the small correction effect takes place and a self-similar solution of the linearized perturbation equation is found, which gives an analytical expression of the correction terms. The result shows a good agreement with the experiments.

In the chapter 7, the experimental procedures are briefly presented, though they are quite routine. Comparisons of the experimental and theoretical results and some discussions will be also included here.

Finally we would like to mention a close relationship of this analysis with the lift contribution to the sonic boom phenomenon. Usually the strength of the sonic boom caused by lifting force of supersonically flying aircraft is calculated by the ray-shock theory based on the geometrical acoustics or the weak blast wave theory (see for example [*12*]), in which no interaction between each ray tube is assumed. This implies there is no boom energy diversion from the stronger ray tubes (downward direction) to the weaker ray tubes (horizontal direction). However, our analysis clearly suggests that this diversion of the boom energy due to the mixing effect may be considerable. This effect should be interesting, because the boom caused by the lifting force is only unmanageable component of the sonic boom energy (those caused by a symmetrical configuration could be cancelled by suitable body configuration, at least in principle). Recent experimental data obtained by Bird etc. [*13*] strongly suggest the existence of this effect in a wind tunnel experiment of asymmetrical cone models.

2. The Characteristic Rule

We consider the problem represented in the figure 2 wherein a shock wave initially moves in the straight part of the tube $x<0$, and then passes to the non-uniform part $x>0$, where the area $A(x)$ varies from the original value A_1. The flow ahead of the shock is assumed to be uniform and stationary. Conditions ahead of the shock will be denoted by a subscript 0; subscript 1 denotes the constant values behind the shock, when it is uniform in $x<0$. When the shock meets the area change at $x=0$, disturbances are reflected along the negative characteristics

C_- and entropy changes propagate along the particle paths P. Disturbances on negative characteristics move backwards or forwards relative to the tube depending on whether the flow behind the shock is supersonic or subsonic, respectively.

Generally, one-dimensional, unsteady flow problems are described by the equations of motion

$$\begin{aligned} &\rho_t+u\rho_x+\rho u_x+\frac{\rho u}{A}A_x=0 \\ &\rho u_t+\rho u u_x+p_x=0 \\ &s_t+us_x=0\,, \end{aligned} \tag{2.1}$$

where p is the pressure, ρ is the density, u is the particle velocity, s is the specific entropy, the subscripts t and x denote the partial differentials with respect to t and x, respectively. The effects of viscosity and heat conduction are neglected. From these equations, we find three characteristic lines C_+, C_- and P, which are

$$\begin{aligned} &\frac{dx}{dt}=u+a && \text{on } C_+ \text{ characteristics} \\ &\frac{dx}{dt}=u-a && \text{on } C_- \text{ characteristics} \\ &\frac{dx}{dt}=u\,, && \text{on } P \text{ characteristics} \end{aligned} \tag{2.2}$$

where a is the speed of sound.
In the characteristic forms, we have

$$\{u_t+(u+a)u_x\}+\frac{1}{\rho a}\{p_t+(u+a)p_x\}=-\frac{au}{A}A_x \tag{2.3}$$

$$\{u_t+(u-a)u_x\}-\frac{1}{\rho a}\{p_t+(u-a)p_x\}=-\frac{au}{A}A_x \tag{2.4}$$

$$s_t+us_x=0\,. \tag{2.5}$$

The boundary value problem for this system of differential equations can be set as follows: In the initial undisturbed region, $t<0$, $x<0$, the uniform shock Mach number M_1 and all the other flow conditions are given. On the right of an unknown shock wave, the state of the gas is prescribed by $u_0=0$, $a=a_0$ and $s=s_0$. Along this line compatibility conditions must be fulfilled. These conditions connect the parameters ahead of the shock wave (suffix 0) with those on the back of the shock wave (suffix 2), and can be written in the forms

$$\begin{aligned} u_2&=\frac{2a_0}{\gamma+1}\left(M-\frac{1}{M}\right) \\ p_2&=\frac{p_0}{\gamma+1}(2\gamma M^2-\gamma+1) \\ \rho_2&=\rho_0\frac{(\gamma+1)M^2}{2+(\gamma-1)M^2} \\ a_2&=\frac{a_0}{(\gamma+1)}\frac{\sqrt{(2\gamma M^2-\gamma+1)\{2+(\gamma-1)M^2\}}}{M}\,. \end{aligned} \tag{2.6}$$

In terms of the changes in the shock Mach number, we have

$$du_2=\frac{2a_0}{\gamma+1}\left(1+\frac{1}{M^2}\right)dM$$
$$dp_2=\frac{4\gamma p_0}{\gamma+1}MdM. \tag{2.7}$$

Integrating the equation (2.3) along C_+ characteristics from $x<0$ to the shock front, we obtain

$$\int_{u_1}^{u_2}du+\int_{p_1}^{p_2}\frac{dp}{\rho a}=-\int_{\ln A_1}^{\ln A_2}\frac{au}{a+u}\frac{dA}{A}. \tag{2.8}$$

We now partially differentiate this relation (2.8) with respect to x

$$\frac{du_2}{dx}+\frac{1}{\rho_2 a_2}\frac{dp_2}{dx}+\int_{p_1}^{p_2}\frac{\partial}{\partial x}\left(\frac{1}{\rho a}\right)dp=-\frac{a_2u_2}{a_2+u_2}\frac{d(\ln A_2)}{dx}-\int_{\ln A_1}^{\ln A_2}\frac{\partial}{\partial x}\left(\frac{au}{a+u}\right)d(\ln A). \tag{2.9}$$

For the case where the variations of the flow behind the shock wave are small, we can omitt the two terms in which the integral operations appear as small quantities of the second order.

$$\left\{\frac{2a_0}{\gamma+1}\left(1+\frac{1}{M^2}\right)+\frac{1}{\rho_2a_2}\frac{4\gamma p_0}{(\gamma+1)}M\right\}\frac{dM}{dx}=-\frac{a_2u_2}{a_2+u_2}\frac{1}{A}\frac{dA}{dx}. \tag{2.10}$$

Here we define the decay coefficient D as

$$D=-\frac{A}{M}\frac{dM}{dA},$$

which is given in this case as

$$D=\frac{K}{2}\left(1-\frac{1}{M^2}\right), \tag{2.11}$$

where

$$K^{-1}=\frac{1}{2}\left(1+\frac{2}{\gamma+1}\frac{1-\mu^2}{\mu}\right)\left(2\mu+1+\frac{1}{M^2}\right)$$
$$\mu^2=\frac{(\gamma-1)M^2+2}{2\gamma M^2-(\gamma-1)}.$$

This rule was given by Rościszewski in a slightly different way [8], and also Whitham obtained this rule using the equation (2.3) in which he replaced derivatives in the characteristic direction by derivatives in the shock wave direction $\frac{\partial}{\partial t}+(u+a)\frac{\partial}{\partial x}\simeq\frac{\partial}{\partial t}+aM\frac{\partial}{\partial x}$ [7]. He remarks that the slope of the C_+ characteristics is close to that of the shock wave line (in the linearized approximation, they are the same). The same result can be obtained (Chisnell [6]) by solving first the linearized case for small shock wave velocity variations, and then, for the case of arbitrary variable shock wave velocity, changing the parameter in the linearized solution. The quasi-linearized solution thus obtained, in fact, is the result of applying a series of local linearized solutions to the case where finite

changes in shock wave velocity take place.

Now let us evaluate the omitted terms in (2.10). Putting

$$\begin{aligned}\varepsilon&=\int_{p_1}^{p_2}\frac{\partial}{\partial x}\left(\frac{1}{\rho a}\right)dp\\ \sigma&=\int_{\ln A_1}^{\ln A_2}\frac{\partial}{\partial x}\left(\frac{au}{a+u}\right)d(\ln A)\,,\end{aligned}\tag{2.12}$$

and from (2.10) and (2.11), we have

$$\frac{1}{DM}\frac{dM}{dx}=-\frac{1}{A}\frac{dA}{dx}-\left(\frac{a_2+u_2}{a_2u_2}\right)(\varepsilon+\sigma)\,.\tag{2.13}$$

Therefore, if

$$\left(\frac{1}{a_2}+\frac{1}{u_2}\right)(\varepsilon+\sigma)A\frac{dx}{dA}\ll 1\,,\tag{2.14}$$

then the neglection of these terms is justified.

In order to evaluate the flow quantities behind the shock front, we linearize the equations (2.3) (2.4) and (2.5),

$$\begin{aligned}(p-p_1)+\rho_1a_1(u-u_1)&=-\frac{\rho_1a_1^2u_1}{u_1+a_1}\frac{A-A_1}{A_1}+2F\{x-(u_1+a_1)t\}\\ (p-p_1)-\rho_1a_1(u-u_1)&=-\frac{\rho_1a_1^2u_1}{u_1-a_1}\frac{A-A_1}{A_1}+2G\{x-(u_1-a_1)t\}\\ (\rho-\rho_1)-\frac{1}{a_1^2}(p-p_1)&=H(x-u_1t)\,,\end{aligned}\tag{2.15}$$

where F gives the disturbance on C_+, G the disturbance on C_-, and H the disturbance on P, respectively. Since the shock was assumed to come undisturbed from $x=-\infty$, the value of F vanishes. The perturbation solutions are, therefore,

$$\begin{aligned}p-p_1&=G\{x-(u_1-a_1)t\}-\frac{\rho_1u_1^2a_1^2}{u_1^2-a_1^2}\frac{A-A_1}{A_1}\\ u-u_1&=-\frac{1}{\rho_1a_1}G\{x-(u_1-a_1)t\}+\frac{u_1a_1^2}{u_1^2-a_1^2}\frac{A-A_1}{A_1}\\ \rho-\rho_1&=\frac{1}{a_1^2}(p-p_1)+H(x-u_1t)\,.\end{aligned}\tag{2.16}$$

At the shock front, we have the linearized Rankine-Hugoniot relations

$$\begin{aligned}p-p_1&=\frac{4\gamma p_0}{\gamma+1}M_1(M-M_1)\\ u-u_1&=\frac{2a_0}{\gamma+1}\left(1+\frac{1}{M_1^2}\right)(M-M_1)\\ \rho-\rho_1&=\frac{4(\gamma+1)p_0M_1}{\{2+(\gamma-1)M_1^2\}^2}(M-M_1)\,.\end{aligned}\tag{2.17}$$

Substituting the conditions at the shock (2.17) into (2.16) at $t=x/U_1$, where U is the speed of the shock wave, we have

$$\frac{2}{\left(1-\frac{1}{M_1^2}\right)K_1}\frac{(M-M_1)}{M_1}=-\frac{A-A_1}{A_1} \tag{2.18}$$

$$\begin{aligned} G\left(\frac{x}{k_2}\right)&=-\frac{\rho_1 u_1^2 a_1^2}{a_1^2-u_1^2}k_1\frac{A-A_1}{A_1}\\ H\left(\frac{x}{k_3}\right)&=k_4\frac{A-A_1}{A_1}, \end{aligned} \tag{2.19}$$

where

$$\begin{aligned} \frac{1}{K_1}&=\frac{1}{2}\left(1+\frac{u_1}{a_1}\right)\left(1+2\mu+\frac{1}{M_1^2}\right)\\ \mu_1^2&=\frac{(\gamma-1)M_1^2+2}{2\gamma M_1^2-(\gamma-1)}\\ k_1&=1+\frac{a_1^2-u_1^2}{u_1 a_1}\mu_1 K_1\\ k_2&=\frac{U_1}{U_1-u_1+a_1}\\ k_3&=\frac{U_1}{U_1-u_1}\\ k_4&=\frac{\gamma-1}{2}\frac{u_1^2}{a_1^2}\rho_1 K_1\left(1-\frac{1}{M_1^2}\right). \end{aligned}$$

Equation (2.18) gives the change in the shock Mach number, which, naturally, corresponds to the linearized form of (2.10). From (2.16), (2.18) and (2.19), the full solution of the flow field behind the shock is

$$\begin{aligned} p-p_1&=-\frac{\rho_1 u_1^2 a_1^2}{a_1^2-u_1^2}\left\{k_1\frac{A\{k_2[x-(u_1-a_1)t]\}-A_1}{A_1}-\frac{A(x)-A_1}{A_1}\right\}\\ u-u_1&=\frac{u_1 a_1^2}{a_1^2-u_1^2}\left\{\frac{u_1}{a_1}k_1\frac{A\{k_2[x-(u_1-a_1)t]\}-A_1}{A_1}-\frac{A(x)-A_1}{A_1}\right\}\\ \rho-\rho_1&=\frac{1}{a_1^2}(p-p_1)+k_4\frac{A\{k_3(x-u_1t)\}-A_1}{A_1}\\ a-a_1&=-\frac{\gamma(\gamma-1)u_1^2}{4a_1}K_1\left(1-\frac{1}{M_1^2}\right)\frac{A\{k_3(x-u_1t)\}-A_1}{A_1}. \end{aligned} \tag{2.20}$$

This is Chester's solution [5]. As seen in the equation (2.20), the solution breaks down near sonic condition when $u_1=a_1$. This point was improved by Friedman finding a higher order linearized solution [9], but there is no room left open for further discussions on this point. However, it is interesting to note that this solution gives a convergence of C_- characteristics —a secondary shock wave— as schematically shown in Fig. 2, which is actually observed in the experiment.

Using this solution, the omitted terms are expressed as

$$\varepsilon=-\int_{p_1}^{p_2}\left(\frac{1}{\rho_1 a_1^2}\frac{\partial a}{\partial x}+\frac{1}{\rho_1^2 a_1}\frac{\partial \rho}{\partial x}\right)dp$$

$$\sigma=\int_{\ln A_1}^{\ln A_2}\frac{u_2^1\dfrac{\partial a}{\partial x}+a_1^2\dfrac{\partial u}{\partial x}}{(a_1+u_1)^2}d(\ln A)\,. \tag{2.21}$$

Here, for simplicity of the calculation, we assume that the area A is proportional to x, that is, the channel is a part of cylindrically expanding flow starting at $x=x_1$, then we have

$$\frac{1}{A_1}\frac{dA}{dx}=\frac{1}{x_1} \tag{2.22}$$

and

$$\begin{aligned}
\frac{\partial a}{\partial x}&=-\frac{\gamma(\gamma-1)u_1^2K_1\left(1-\dfrac{1}{M_1^2}\right)k_3}{4a_1}\frac{1}{x_1}\\
\frac{\partial u}{\partial x}&=\frac{u_1a_1^2}{a_2^1-u_1^2}\left\{\frac{u_1}{a_1}k_1k_2-1\right\}\frac{1}{x_1}\\
\frac{\partial \rho}{\partial x}&=\left\{-\frac{\rho_1u_1^2}{a_1^2-u_1^2}(k_1k_2-1)+k_3k_4\right\}\frac{1}{x_1}\,,
\end{aligned} \tag{2.23}$$

finally

$$\begin{aligned}
\varepsilon&=\left\{\frac{\gamma(\gamma-1)u_1^2K_1\left(1-\dfrac{1}{M_1^2}\right)k_3}{4\rho_1a_1^3}+\frac{1}{\rho_1a_1}\left[\frac{u_1^2(k_1k_2-1)}{a_1^2-u_1^2}-k_3k_4\right]\right\}\frac{p_2-p_1}{x_1}\\
\sigma&=\left[-\frac{\gamma(\gamma-1)u_1^4K_1\left(1-\dfrac{1}{M_1^2}\right)k_3}{4a_1(a_1+u_1)^2}+\frac{u_1a_1^4\left\{\dfrac{u_1}{a_1}k_1k_2-1\right\}}{(a_1+u_1)^2(a_1^2-u_1^2)}\right]\frac{\ln A_2/A_1}{x_1}\,.
\end{aligned} \tag{2.24}$$

Thus, the criterion (2.14) is transformed into

$$\left(\frac{1}{a_1}+\frac{1}{u_1}\right)(\varepsilon+\sigma)x_1\ll 1\,. \tag{2.25}$$

Now, let us find out the numerical value corresponding to $M=\infty$ since this is one of the most critical cases. For $M=\infty$, we have

$$\begin{aligned}
&u=\frac{2a_0}{\gamma+1}M\,,\quad p=\frac{2\gamma p_0}{\gamma+1}M^2\,,\quad \rho=\rho_0\frac{\gamma+1}{\gamma-1}\,,\\
&a=\frac{a_0\sqrt{2\gamma(\gamma-1)}}{\gamma+1}M\,,\\
&\mu_1=\sqrt{\frac{\gamma-1}{2\gamma}}\,,\quad K_1=\frac{2\gamma\sqrt{\gamma-1}}{\{\sqrt{2}+\sqrt{\gamma(\gamma-1)}\}\{\sqrt{\gamma}+\sqrt{2(\gamma-1)}\}}\,,\\
&k_1=1+\frac{(\gamma-2)(\gamma+1)}{2\gamma}K_1\,,\quad k_2=\frac{\gamma+1}{\gamma-1+\sqrt{2\gamma(\gamma-1)}}\,,\quad k_3=\frac{\gamma+1}{\gamma-1}\,,\\
&k_4=\frac{\rho_0(\gamma+1)}{\gamma(\gamma-1)}K_1\,,
\end{aligned} \tag{2.26}$$

and the criterion is

$$\left(\frac{1}{a_1}+\frac{1}{u_1}\right)(\varepsilon+\sigma)x_1\sim\frac{1}{M_1}\ln\frac{A_2}{A_1}. \tag{2.27}$$

Thus this characteristic rule is well justified provided with the small change of area.

3. The Weak Blast Wave Theory

As discussed in the previous chapter and the introduction, the characteristic rule is no longer applicable, if the area change is large or if the constant upstream part disappears forming secondary shocks or discontinuities—a center core. For such case, the weak blast wave theory is useful since it takes into consideration the local flow pattern in the neighbourhood of the shock front. Here we derive an $A-M$ relation using this theory.

The equations for conservations of mass, momentum and energy along a ray tube are given in the equation (2.1), for convenience' sake, they are rewritten here as follows:

$$\begin{aligned}
&\rho_t+u\rho_x+\rho u_x+\frac{\rho u}{A}A_x=0\\
&u_t+uu_x+\frac{1}{\rho}p_x=0\\
&p_t+up_x+a^2\rho u_x+\frac{\rho u a^2}{A}A_x=0\,.
\end{aligned} \tag{3.1}$$

The solution of these equations will be assumed to take the forms of a perturbation on the undisturbed conditions

$$\begin{aligned}
u&=u^{(1)}\left(t-\frac{x}{a_0}\right)+u^{(2)}\left(t-\frac{x}{a_0}\right)^2+\cdots\\
p&=p_0+p^{(1)}\left(t-\frac{x}{a_0}\right)+p^{(2)}\left(t-\frac{x}{a_0}\right)^2+\cdots\\
\rho&=\rho_0+\rho^{(1)}\left(t-\frac{x}{a_0}\right)+\rho^{(2)}\left(t-\frac{x}{a_0}\right)^2+\cdots\,.
\end{aligned} \tag{3.2}$$

Derivatives of these functions take the following forms;

$$\begin{aligned}
u_t&=u^{(1)}+2u^{(2)}\left(t-\frac{x}{a_0}\right)+\cdots\\
u_x&=-\frac{1}{a_0}u^{(1)}+\left(u_x^{(1)}-\frac{2}{a_0}u^{(2)}\right)\left(t-\frac{x}{a_0}\right)+\cdots\\
p_t&=p^{(1)}+2p^{(2)}\left(t-\frac{x}{a_0}\right)+\cdots\\
p_x&=-\frac{1}{a_0}p^{(1)}+\left(p_x^{(1)}-\frac{2}{a_0}p^{(2)}\right)\left(t-\frac{x}{a_0}\right)+\cdots\\
\rho_t&=\rho^{(1)}+2\rho^{(2)}\left(t-\frac{x}{a_0}\right)+\cdots\\
\rho_x&=-\frac{1}{a_0}\rho^{(1)}+\left(\rho_x^{(1)}-\frac{2}{a_0}\rho^{(2)}\right)\left(t-\frac{x}{a_0}\right)+\cdots\,.
\end{aligned} \tag{3.3}$$

Substituting these expressions into (3.1), one obtains for the zeroth order equations

$$\begin{aligned} \rho^{(1)} &= \frac{\rho_0}{a_0} u^{(1)} \\ p^{(1)} &= \frac{\gamma p_0}{a_0} u^{(1)} . \end{aligned} \tag{3.4}$$

The first order terms of $(t-x/a_0)$ yield

$$\begin{aligned} &2\rho^{(2)} - \frac{2\rho_0}{a_0} u^{(2)} + \rho_0 u_x^{(1)} + \rho_0 \frac{A_x}{A} u^{(1)} - \frac{2}{a_0} u^{(1)} p^{(1)} = 0 \\ &2\rho_0 u^{(2)} - \frac{2}{a_0} p^{(2)} + p_x^{(1)} + \rho^{(1)} u^{(1)} - \frac{\rho_0}{a_0} u^{(1)2} = 0 \\ &2p^{(2)} - \frac{2\gamma p_0}{a_0} u^{(2)} + \gamma p_0 u_x^{(1)} + \gamma p_0 u^{(1)} \frac{A_x}{A} - \frac{(\gamma-1)}{a_0} p^{(1)} u^{(1)} = 0 . \end{aligned} \tag{3.5}$$

Eliminating the terms of $p^{(2)}$ and $u^{(2)}$ from the second and third equations of (3.5) and using (3.4), one obtains

$$2u_x^{(1)} + u^{(1)} \frac{A_x}{A} - (\gamma+1) \frac{u^{(1)2}}{a_0^2} = 0 . \tag{3.6}$$

Here, if we neglect the non-linear term $(\gamma+1)u^{(1)2}/a_0^2$, the result is

$$u^{(1)} \propto \frac{1}{\sqrt{A}} . \tag{3.7}$$

This is a well-known result of the geometrical acoustics. However, the equation (3.6) is easily integrated to

$$u^{(1)} = -\frac{2a_0^2}{\gamma+1} \frac{1}{\sqrt{A} \int_0^x \frac{dx}{\sqrt{A}}} . \tag{3.8}$$

This relates the perturbation strength to the distance along the tube. As the shock moves from the source the cumulative effect of the expansion wave behind the shock wave is felt. This is what causes the attenuation represented by the integral in the equation (3.8). Far downstream this term may predominate and the geometrical acoustics may fail to be useful.

Next, we assume the shock location to being expressed

$$t - \frac{x}{a_0} + l = 0 . \tag{3.9}$$

The quantity $l(x)$ is the correction of the present theory over the acoustic theory. Then, differentiating (3.9) with respect to x, the Mach number of the shock front M is given

$$\frac{1}{M} = 1 - a_0 l_x . \tag{3.10}$$

On the other hand, from the Rankine-Hugoniot relations, we have

$$u_2 = \frac{2a_0}{\gamma+1} \left(M - \frac{1}{M} \right) \tag{3.11}$$

and, from the definition

$$u_2=u^{(1)}\left(t-\frac{x}{a_0}\right)+\cdots\doteq -u^{(1)}l\,. \tag{3.12}$$

Using (3.6), (3.10), (3.11) and (3.12), the following decay rule is derived

$$\left(\frac{M^2+1}{M^2-1}\right)\frac{dM}{Mdx}+\frac{1}{2}\frac{dA}{Adx}+\frac{M}{M+1}\frac{1}{\sqrt{A}\int_0^x\frac{dx}{\sqrt{A}}}=0 \tag{3.13}$$

The decay coefficient D is given in this case as

$$D=-\frac{A}{M}\frac{dM}{dA}=\frac{1}{2}\left(\frac{M^2-1}{M^2+1}\right)\left(1+\frac{2M}{M+1}\frac{\sqrt{A}}{\int_0^x\frac{dx}{\sqrt{A}}\frac{dA}{dx}}\right) \tag{3.14}$$

This will be called the decay coefficient in the weak blast wave theory.

In the process of this deduction, a weak shock approximation usually takes place, that is, (3.11) is approximated by

$$u_2=\frac{4a_0}{\gamma+1}\left(1-\frac{1}{M}\right), \tag{3.15}$$

then from (3.10) and (3.12)

$$\frac{l}{2\sqrt{A}\int\frac{dx}{\sqrt{A}}}=l_x \tag{3.16}$$

This is integrated to

$$l\propto\int\frac{dx}{\sqrt{A}}\,. \tag{3.17}$$

The decay rule in this approximation is

$$\frac{1}{(M-1)M}\frac{dM}{dx}+\frac{1}{2}\frac{1}{A}\frac{dA}{dx}+\frac{1}{2}\frac{1}{\sqrt{A}\int\frac{dx}{\sqrt{A}}}=0 \tag{3.18}$$

or

$$D=-\frac{AdM}{MdA}=\frac{1}{2}(M-1)\left(1+\frac{\sqrt{A}}{\int\frac{dx}{\sqrt{A}}\cdot\frac{dA}{dx}}\right) \tag{3.19}$$

This will be called the decay coefficient in the simplified weak blast wave theory.

On the other hand, since under the geometrical acoustics, $l=$constant, we have

$$D=-\frac{AdM}{MdA}=\frac{1}{2}(M-1)\,. \tag{3.20}$$

This will be called the decay coefficient in the geometrical acoustics.

Before proceeding further, let us assume the form $A=x^j$, then $j=1$ corresponds to a cylindrical wave, $j=2$ to a spherical wave and $j=0$ to a plane wave, respectively. Then

$$\frac{\sqrt{A}}{\int \frac{dx}{\sqrt{A}} \cdot \frac{dA}{dx}} = \frac{2-j}{2j} \tag{3.21}$$

and the decay coefficients for $j=1$ are calculated as follows:

$$D=\frac{1}{2}\left(\frac{M^2-1}{M^2+1}\right)\left(1+\frac{M}{M+1}\right)$$

in the weak blast wave theory

$$D=\frac{3}{4}(M-1)$$

in the simplified weak blast wave theory

$$D=\frac{1}{2}(M-1)$$

in the geometrical acoustics.

The ray tube geometry in our ray-shock analysis may be most suitably approximated by $j=1$ and occasionally it may take the smaller value of j, which means larger value of D, but it hardly gets the larger value than 1, since the flow pattern is two-dimensional. Then it is noted that the decay coefficient given for $j=1$ may represent the lowest value, corresponding to the lowest attenuation of the shock front. Those decay coefficients and one calculated by (2.11) are presented in Fig. 5, in which possible corrections are also shown. Note that there is a lower limit of the possible decay coefficients calculated under the one-dimensional channel flow analyses.

4. The Ray-Shock Theory

We now discuss the ray-shock theory. The basic equations are reproduced here for convenience' sake

$$\begin{aligned} \theta_\eta &= \frac{1}{M} A_\xi \\ \theta_\xi &= -\frac{1}{A} M_\eta , \end{aligned} \tag{4.1}$$

and

$$D=-\frac{A}{M}\frac{dM}{dA}. \tag{4,2}$$

Substituting (4.2) into (4.1), we have

$$\begin{aligned} M_\xi + \frac{M^2 D}{A}\theta_\eta &= 0 \\ \theta_\xi + \frac{1}{A} M_\eta &= 0 , \end{aligned} \tag{4.3}$$

where the suffices ξ and η mean the partial derivatives with respect to ξ and η, respectively. The flow pattern is schematically shown in Fig. 1 in the physical plane

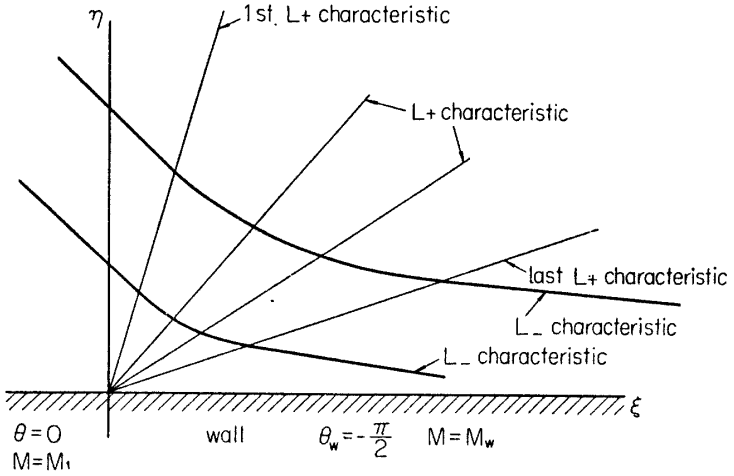

FIGURE 4. Schematic diagram in the ray-shock plane.

and in Fig. 4 in the ray-shock plane. The boundary conditions are easily seen in the figures. The equations (4.3) are a system of quasi-linear homogeneous equations with two variables, so there are two characteristics provided with $D>0$. They are called L_+ and L_- characteristics, respectively, and

$$\begin{aligned} &\frac{d\eta}{d\xi}=\frac{M\sqrt{D}}{A} && L_+ \text{ characteristics} \\ &\frac{d\eta}{d\xi}=-\frac{M\sqrt{D}}{A} && L_- \text{ characteristics.} \end{aligned} \tag{4.4}$$

In the physical plane, they are transformed into

$$\begin{aligned} &\frac{dy}{dx}=\tan(\theta+m) && L_+ \text{ characteristics} \\ &\frac{dy}{dx}=-\tan(\theta+m) && L_- \text{ characteristics,} \end{aligned} \tag{4.5}$$

where

$$\tan m=\sqrt{D}.$$

The characteristic forms of the original equations (4.3) are

$$\theta_\xi+\frac{M\sqrt{D}}{A}\theta_\eta+\frac{1}{M\sqrt{D}}\left(M_\xi+\frac{M\sqrt{D}}{A}M_\eta\right)=0 \tag{4.6}$$

$$\theta_\xi-\frac{M\sqrt{D}}{A}\theta_\eta-\frac{1}{M\sqrt{D}}\left(M_\xi-\frac{M\sqrt{D}}{A}M_\eta\right)=0. \tag{4.7}$$

All the L_- characteristics start at the initial undisturbed region, so the disturbed flow field is described by simple waves. Furthermore, all the disturbed L_+ characteristics start at a point $(x=y=0)$ or $(\xi=\eta=0)$, so they form centered simple waves. Integrating the equation (4.7) along L_- characteristics from the undisturbed region $(\theta=0,\ M=M_1)$ toward the wall, we obtain

$$\theta=\int_{M_1}^{M}\frac{dM}{\sqrt{D}M} \tag{4.8}$$

on all the L_- characteristics, so in everywhere in the simple wave region. This

relation immediately gives the relation between θ and M, especially the diffracted shock wave Mach number M_w along the wall as follows:

$$\theta_w=\int_{M_1}^{M_w}\frac{dM}{\sqrt{D}M} \tag{4.9}$$

where the suffix w means the values along the wall after the diffraction. Similarly, along the L_+ characteristics

$$\theta+\int\frac{dM}{\sqrt{D}M}=\text{constant}. \tag{4.10}$$

Combined with (4.8), we have

$$\theta=\text{constant} \tag{4.11}$$

$$\int\frac{dM}{\sqrt{D}M}=\text{constant} \tag{4.12}$$

along every L_+ characteristic, then all the variables A, M, D and θ are constants along every L_+ characteristic, so the functions of the single quantity η/ξ. The L_+ characteristics are given as

$$\eta=\frac{M\sqrt{D}}{A}\xi. \tag{4.13}$$

In the physical plane, they are

$$Y=X\tan(\theta+m). \tag{4.14}$$

The flow features of this case will be as shown in the figures 1 and 4 where the radial lines started at the corner points correspond to the L_+ characteristics and on each of them M and θ are constants. This centered simple wave region covers the fan formed in the ray-shock plane by

$$\frac{M_1\sqrt{D_1}}{A_1}>\frac{\eta}{\xi}>\frac{M_w\sqrt{D_w}}{A_w}, \tag{4.15}$$

and in the physical plane by

$$\tan m_1>\frac{Y}{X}>\tan(\theta_w+m_w). \tag{4.16}$$

The first disturbance spreads out in the ray-shock plane at a rate given by $M_1\sqrt{D_1}/A_1$. Here we choose η as the value of distance Y from the wall in the initial undisturbed motion so that $A_1=1$.

Thus we obtain the expressions of all the flow quantities. For convenience' sake, they are summarized here

$$\begin{aligned}\frac{\eta}{\xi}&=\frac{M\sqrt{D}}{A}\\ D&=-\frac{A}{M}\frac{dM}{dA}\\ \theta&=\int_{M_1}^{M}\frac{dM}{\sqrt{D}M}\end{aligned} \tag{4.17}$$

in the region of

$$\frac{M_1\sqrt{D_1}}{A_1}>\frac{\eta}{\xi}>\frac{M_w\sqrt{D_w}}{A_w}.$$

The coordinates of the shock front (X, Y), on which $\xi=$constant, are given as

$$\begin{aligned} X&=-\int A\sin\theta\, d\eta \\ Y&=\int A\cos\theta\, d\eta . \end{aligned} \tag{4.18}$$

If we use the characteristic rule (2.11) and assume the value of K, in a practical point of view, to be constant, we have

$$\begin{aligned} D&=\frac{K}{2}\left(1-\frac{1}{M^2}\right) \\ A&=\left(\frac{M_1^2-1}{M^2-1}\right)^{\frac{1}{K}} \\ \frac{\eta}{\xi}&=\sqrt{\frac{K}{2}}\,\frac{(M^2-1)^{\frac{1}{K}+\frac{1}{2}}}{(M_1^2-1)^{\frac{1}{K}}} \\ \frac{M}{M_1}&=\cosh\sqrt{\frac{K}{2}}\theta+\sqrt{1-\frac{1}{M_1^2}}\sinh\sqrt{\frac{K}{2}}\theta \\ \frac{X}{M_1\xi}&=\cos\theta\cdot\cosh\sqrt{\frac{K}{2}}\theta-\sqrt{\frac{K}{2}}\sin\theta\cdot\sinh\sqrt{\frac{K}{2}}\theta \\ &\quad+\sqrt{1-\frac{1}{M_1^2}}\left\{\cos\theta\cdot\sinh\sqrt{\frac{K}{2}}\theta-\sqrt{\frac{K}{2}}\sin\theta\cdot\cosh\sqrt{\frac{K}{2}}\theta\right\} \\ \frac{Y}{M_1\xi}&=\sin\theta\cdot\cosh\sqrt{\frac{K}{2}}\theta-\sqrt{\frac{K}{2}}\cos\theta\cdot\sinh\sqrt{\frac{K}{2}}\theta \\ &\quad+\sqrt{1-\frac{1}{M_1^2}}\left\{\cos\theta\cdot\sinh\sqrt{\frac{K}{2}}\theta-\sqrt{\frac{K}{2}}\sin\theta\cdot\cosh\sqrt{\frac{K}{2}}\theta\right\}, \end{aligned} \tag{4.19}$$

where K takes the values between $^1/_2$ (at $M_1=1$) and 0.394 (for $\gamma=1.4$, $M_1=\infty$). It should be noted that $X/M_1\xi$ and $Y/M_1\xi$ are functions of the single quantity η/ξ, so that the shock pattern expands uniformly with time, and the contribution of the initial Mach number M_1 is not large except for weak shocks.

For the case of $M_1=\infty$, these are simplified as follows:

$$\begin{aligned} D&=\frac{K}{2} \\ A&=\left(\frac{M_1}{M}\right)^{\frac{2}{K}} \\ \frac{\eta}{\xi}&=\sqrt{\frac{K}{2}}\left(\frac{M}{M_1}\right)^{\frac{2}{K}}M \\ \frac{M}{M_1}&=e^{\sqrt{\frac{K}{2}}\theta} \end{aligned} \tag{4.20}$$

$$\frac{X}{M_1\xi}=\left(\cos\theta-\sqrt{\frac{K}{2}}\sin\theta\right)e^{\sqrt{\frac{K}{2}}\theta}$$

$$\frac{Y}{M_1\xi}=\left(\sin\theta+\sqrt{\frac{K}{2}}\cos\theta\right)e^{\sqrt{\frac{K}{2}}\theta},$$

and for $M_1=1$, we have

$$\begin{aligned} D&=\frac{1}{2}\frac{M-1}{M^2}\\ A&=\left(\frac{M_1-1}{M-1}\right)^2\\ \frac{\eta}{\xi}&=\frac{1}{\sqrt{2}}\frac{(M-1)^{5/2}}{(M_1-1)^2}\\ \theta&=2^{3/2}\{\sqrt{M-1}-\sqrt{M_1-1}\}. \end{aligned} \tag{4.21}$$

If we use the result of the simplified weak blast wave theory as a decay rule, we have

$$\begin{aligned} D&=\frac{3}{4}(M-1)\\ \theta&=\frac{4}{\sqrt{3}}(\tan^{-1}\sqrt{M-1}-\tan^{-1}\sqrt{M_1-1}). \end{aligned} \tag{4.22}$$

Those values of M/M_1 are shown in Fig. 6, in which typical experimental data are also included. As easily seen in the equation (4.9), the higher value of D (the stronger attenuation of the shock strength) implies the lower diffracted shock wave strength (the lower M_w/M_1). The experimental data show the higher diffracted shock Mach number, that is, lesser attenuation through expansion, in all the case, especially for the weaker shock waves. Therefore, by this theory of ray-tube, it is impossible to obtain the correct diffraction pattern regardless what kind of decay rule could be adopted, since, as shown in Fig. 5, all the possible decay coefficients are lower than those used here. In other words, the actual diffracted wave shows such low attenuation that any reasonable theory fails to predict. This strongly suggests that the energy or momentum transfer between the ray

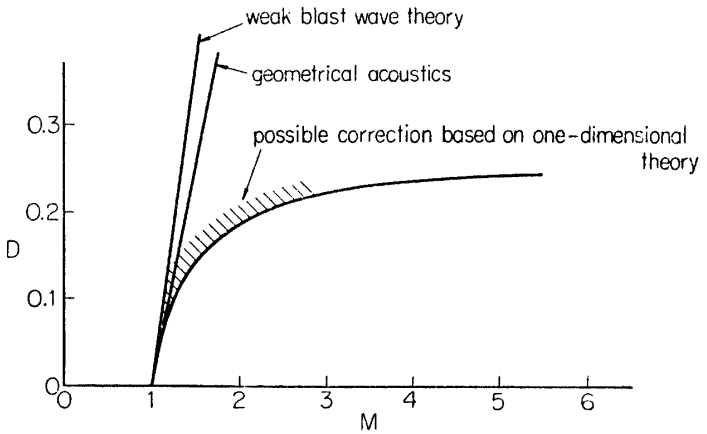

FIGURE 5. Decay coefficients.

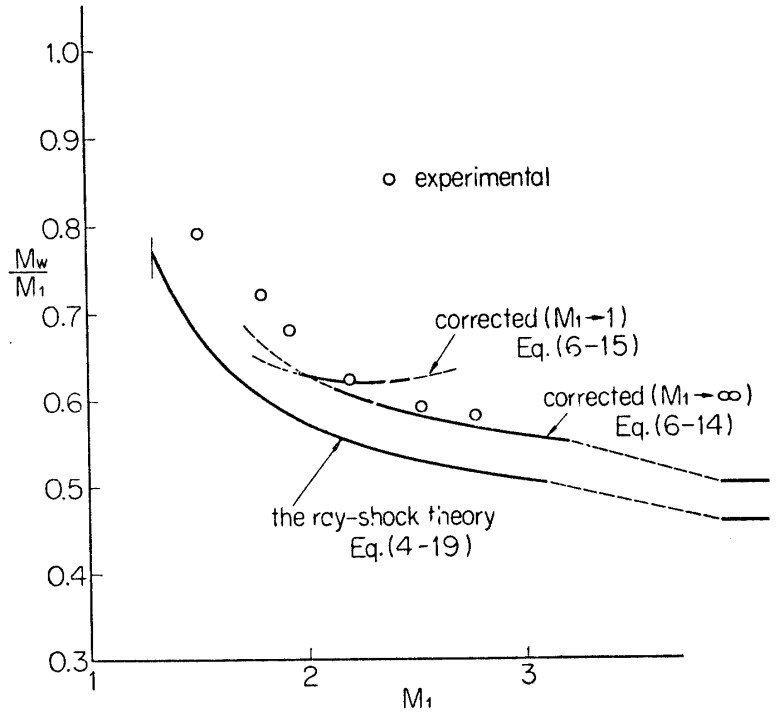

FIGURE 6. Mach numbers of the diffracted shock wave.

tubes should play an important role in this phenomenon. In the next section, let us consider this point.

5. THE GENERALIZED CHARACTERISTIC RULE

From the previous discussions, we find that the discrepancy between the experimental data and the analytical calculations cannot be reasonably explained by any corrections derived from the one-dimensional flow considerations without interaction with the neighbouring ray tubes or the surrounding walls. It must come from the interactions between the neighbouring tubes, that is, the mass, energy or momentum transfer through the ray tube walls due to the viscosity, turbulent mixing, heat conduction, diffusion or caused by the curvature of the ray tubes. The divergence between the ray tubes and the actual particle paths must be considered also. From these considerations, the basic equation (2.1) shall be modified into

$$\begin{aligned} &\rho_t+u\rho_x+\rho u_x=-\rho u\frac{A_x}{A}+m \\ &u_t+uu_x+\frac{1}{\rho}p_x=\frac{1}{\rho}\tau_y+\frac{1}{\rho}g \\ &s_t+us_x=\frac{q}{\rho T}, \end{aligned} \tag{5.1}$$

where m is the mass addition per unit volume, per unit time and shows the effects of the divergence of the ray tubes and the particle paths and the diffussion convection of the mass, τ is the shear stress, which will be discussed later, g is the

body force per unit volume per unit time such as the gravity force or the electromagnetic force, q is the heat addition per unit time per unit volume caused by the viscus dissipation and the heat conduction and the work done by the external force.

Now, the previous studies clearly show that the effects of the upstream flow, i.e. this divergence and curvature of the ray tubes and any interactions taking place in the upstream portion, may not be important. Therefore the most predominant effect must be found in the neighbourhood of the shock front. Since the particle paths intersect perpendicularly to the wave front, then, only the predominant effect must be the shear stress between the neighbouring tubes immediately behind the shock front. Based on these considerations, we retain only the shear stress term into the unsteady one-dimensional flow equations (5.1), then we obtain

$$\begin{aligned} &\rho_t+u\rho_x+\rho u_x+\rho u\frac{A_x}{A}=0\\ &u_t+uu_x+\frac{1}{\rho}p_x=\frac{1}{\rho}\tau_y \qquad (5.2)\\ &s_t+us_x=0\,. \end{aligned}$$

The shear stress τ consists of viscus shear stress and Reynolds stress, if the flow is turbulent. Numerical estimation shows the viscus force is too small to give any measureable effect on the flow pattern. Then we have to recall the Reynolds stress in order to explain the strong interaction between the ray tubes observed experimentally, although we have no direct evidence that the turbulent mixing does take place immediately behind the shock front. However, the strong density variation around the corner observed in the interferograms may positively support this prediction. Now, in the theory of the turbulent mixing we have three hypothetical theories, which are Prandtle's momentum transfer theory, Taylor's vorticity transfer theory and Karman's dynamical similarity theory. In our condition, the predominant feature of the flow is the mixing of the vorticity produced by the curved shock wave which is essentially two-dimensional. Furthermore, it is quite natural to suppose that the flow mixing immediately behind the shock front is similar regardless of the position of the shock front. Therefore we will adopt the vorticity transfer theory and the dynamical similarity theory, by which the shear stress is expressed as

$$\tau=\rho l_v^2\left(\frac{du}{dy}\right)^2=\rho\kappa^2\frac{\left(\frac{du}{dy}\right)^3\left|\frac{du}{dy}\right|}{\left(\frac{d^2u}{dy^2}\right)^2} \qquad (5.3)$$

$$\tau_y=2\rho l_v\left|\frac{du}{dy}\right|\frac{d^2u}{dy}=2\rho\kappa^2\frac{\left(\frac{du}{dy}\right)^2\left|\frac{du}{dy}\right|}{\frac{d^2u}{dy}}, \qquad (5.4)$$

where l_v is the mixing length and κ is a constant determined by experiments. It

is worthwhile to note here that these mixing theories are well-established for the incompressible turbulent flow, although we have had no conclusive result for the compressible turbulent flow yet. The value of κ obtained experimentally in the incompressible turbulent flow is about 0.4.

These equations (5.2) are a system of quasi-linear non-homogeneous hyperbolic partial differential equations with respect to t and x. Then we will follow the similar process as in the chapter 2. Firstly, they have the same characteristic equations as (2.2), and we have the characteristic forms

$$u_t+(u+a)u_x+\frac{1}{\rho a}\{p_t+(u+a)p_x\}=-\frac{au}{A}A_x+\frac{\tau_y}{\rho} \tag{5.5}$$

$$u_t+(u-a)u_x-\frac{1}{\rho a}\{p_t+(u-a)p_x\}=\frac{au}{A}A_x+\frac{\tau_y}{\rho} \tag{5.6}$$

$$s_t+us_x=0. \tag{5.7}$$

The equation (5.5) is integrated along C_+ characteristics from the initial undisturbed condition (denoted by suffix 1) up to the position right behind the shock front (denoted by suffix 2)

$$\int_{u_1}^{u_2}du+\int_{p_1}^{p_2}\frac{dp}{\rho a}=-\int_{\ln A_1}^{\ln A_2}\frac{au}{a+u}d(\ln A)+\int_{x_1}^{x_2}\frac{1}{a+u}\frac{\tau_y}{\rho}dx. \tag{5.8}$$

Differentiating the equation (5.8) with respect to x, we have

$$\begin{aligned}&\frac{du_2}{dx}+\frac{1}{\rho_2a_2}\frac{dp_2}{dx}+\int_{p_1}^{p_2}\frac{\partial}{\partial x}\left(\frac{1}{\rho a}\right)dp\\&=-\frac{a_2u_2}{a_2+u_2}\frac{d(\ln A)}{dx}-\int_{\ln A_1}^{\ln A_2}\frac{\partial}{\partial x}\left(\frac{au}{a+u}\right)d(\ln a)\\&\quad+\frac{1}{a_2+u_2}\frac{(\tau_y)_2}{\rho_2}+\int_{x_2}^{x_2}\frac{\partial}{\partial x}\left\{\frac{\tau_y}{(a+u)\rho}\right\}dx.\end{aligned} \tag{5.9}$$

Since the mixing is effective only in the immediate neighbourhood of the shock front, all the terms with integrations will be neglected for the same reason discussed in the chapter 2. Thus we obtain a decay rule

$$\frac{1}{DM}\frac{dM}{dx}=-\frac{1}{A}\frac{dA}{dx}+\frac{(\tau_y)_2}{\rho_2a_2u_2}, \tag{5.10}$$

where D is the same decay coefficient as in (2.11) and the last term expresses the correction term due to the shear stress,

$$\frac{(\tau_y)_2}{\rho_2a_2u_2}=\frac{2\kappa^2(u_y)_2^3}{a_2u_2(u_{yy})_2}. \tag{5.11}$$

Substituting the values given in (2.6), we obtain

$$\frac{(\tau_y)_2}{\rho_2a_2u_2}=\frac{4\kappa^2\left(1+\frac{1}{M^2}\right)M_y^3}{\sqrt{(2\gamma M^2-\gamma+1)\{2+(\gamma-1)M^2\}}\left(1-\frac{1}{M^2}\right)\left\{\left(1+\frac{1}{M^2}\right)M_{yy}-\frac{2}{M^3}M_y^2\right\}}. \tag{5.12}$$

6. The Generalized Ray-Shock Theory

Here we follow the process shown in the chapter 4, which is called the generalized ray-shock theory. Noting that

$$\frac{\partial}{\partial y}=\frac{\partial}{A\partial\eta}\qquad \frac{\partial^2}{\partial y^2}=\frac{1}{A^2}\left(\frac{\partial^2}{\partial\eta^2}-\frac{1}{A}\frac{\partial A}{\partial\eta}\frac{\partial}{\partial\eta}\right)$$
$$\frac{\partial}{\partial x}=\frac{\partial}{M\partial\xi} \tag{6.1}$$

and from (5.10)

$$\frac{1}{DM^2}M_\xi=-\frac{1}{AM}A_\xi+\frac{(\tau_y)_2}{\rho_2 a_2 u_2}, \tag{6.2}$$

we obtain a system of equations, which corresponds to (4.3)

$$\theta_\eta+\frac{A}{DM^2}M_\xi=\frac{A(\tau_y)_2}{\rho_2 a_2 u_1}$$
$$\theta_\xi+\frac{1}{A}M_\eta=0, \tag{6.3}$$

where the shear correction term is given as

$$\frac{A(\tau_y)_2}{\rho_2 a_2 u_2}=\frac{4\kappa^2\left(1+\frac{1}{M^2}\right)^3 M_\eta^3}{\sqrt{(2\gamma M^2-\gamma+1)\{2+(\gamma-1)M^2\}}\left(1-\frac{1}{M^2}\right)\times}$$
$$\times\left[\left(1+\frac{1}{M^2}\right)\left\{M_{\eta\eta}-\frac{1}{A}A_\eta M_\eta\right\}-\frac{2}{M^3}M_\eta^2\right]. \tag{6.4}$$

There is no way to find out a simple solution of this system of the equations, we assume that the shear stress effect is small and represent all the parameters as the sum of parameters corresponding to the simple wave solution stated in the chapter 4 and disturbances caused by the shear stress effect; we write

$$\theta=\theta^0+\theta'$$
$$M=M^0+M'$$
$$\frac{A}{DM^2}=\left(\frac{A}{DM^2}\right)^0+\left(\frac{A}{DM^2}\right)' \tag{6.5}$$
etc.,

where

$$\theta'\ll\theta^0$$
$$M'\ll M^0$$
$$\left(\frac{A}{DM^2}\right)'=\left(\frac{1}{DM^2}\right)^0 A'-\left(\frac{A}{D^2M^2}\right)^0 D'-2\left(\frac{A}{DM^3}\right)^0 M'$$
$$\ll\left(\frac{A}{DM^2}\right)^0.$$

Then we have the equations for the basic simple wave solution,

$$\theta^0_\eta+\left(\frac{A}{DM^2}\right)^0 M^0_\xi=0$$
$$\theta^0_\xi+\left(\frac{1}{A}\right)^0 M^0_\eta=0\,. \tag{6.6}$$

These are the same equations as those solved in the chapter 4.

The perturbation terms give

$$\theta'_\eta+\left(\frac{A}{DM^2}\right)^0 M'_\xi=\left(\frac{A(\tau_y)_2}{\rho_2 a_2 u_2}\right)^0-\left(\frac{A}{DM^2}\right)' M^0_\xi$$
$$\theta'_\xi+\left(\frac{1}{A}\right)^0 M'_\eta=-\left(\frac{1}{A}\right)' M^0_\eta\,, \tag{6.7}$$

where

$$\left(\frac{A(\tau_y)_2}{\rho_2 a_2 u_2}\right)^0=\frac{4\kappa^2\left(1+\frac{1}{M^2}\right)^3}{\xi c_M\sqrt{(2\gamma M^2-\gamma+1)\{2+(\gamma-1)M^2\}}\times}$$
$$\times\left(1-\frac{1}{M^2}\right)\left[\left(1+\frac{1}{M^2}\right)\frac{c_{MM}}{c_M}-\left(1+\frac{1-2D}{M^2}\right)\frac{1}{M}\right], \tag{6.8}$$

as

$$c=\frac{\eta}{\xi}=\left(\frac{M\sqrt{D}}{A}\right)^0$$
$$M^0_\eta=\frac{1}{\xi c_M}\qquad M^0_{\eta\eta}=-\frac{c_{MM}}{\xi^2 c_M^3}\,. \tag{6.9}$$

Let us find out a simple wave solution of the perturbed quantities. Assuming all the variables are functions of a single quantity $\eta/\xi\,(=c)$, then we have the transformed forms of (6.7) as

$$\theta'_c-\left(\frac{A}{DM^2}\right)^0 cM'_c=S+\left(\frac{A}{DM^2}\right)' cM^0_c$$
$$-c\theta'_c+\left(\frac{1}{A}\right)^0 M'_c=-\left(\frac{1}{A}\right)' M^0_c\,, \tag{6.10}$$

where

$$S=\frac{4\kappa^2\left(1+\frac{1}{M^2}\right)^3}{c_M\sqrt{(2\gamma M^2-\gamma+1)\{2+(\gamma-1)M^2\}}\left(1-\frac{1}{M^2}\right)\times}$$
$$\times\left[\left(1+\frac{1}{M^2}\right)\frac{c_{MM}}{c_M}-\left(1+\frac{1-2D}{M^2}\right)\frac{1}{M}\right]. \tag{6.11}$$

These relations immediately give

$$\left(\frac{A}{DM^2}\right)' c^2-\left(\frac{1}{A}\right)'=-Sc_M c\,. \tag{6.12}$$

Using the relation (4.19), we can easily obtain the correction term M' as

$$M'=\frac{\sqrt{2K}\kappa^2(M^2-1)^{1/2}(M^2+1)^3}{\left(1+\frac{2}{K}\right)M^5\sqrt{(2\gamma M^2-\gamma+1)\{2+(\gamma-1)M^2\}}} \times\frac{1}{\left[\left(\frac{2}{K}-1\right)\frac{M^2+1}{M(M^2-1)}+\frac{K}{M^2}\left(1-\frac{1}{M^2}\right)\right]}. \tag{6.13}$$

Fro the case of $M_1\sim\infty$, this relation is simplified to, for $\gamma=1.4$,

$$M'=\frac{\sqrt{K}\kappa^2M}{\sqrt{\gamma(\gamma-1)}\left\{\left(\frac{2}{K}\right)^2-1\right\}}=0.0338k^2M. \tag{6.14}$$

For the case of $M_1\sim1$, we have, for $\gamma=1.4$,

$$M'=\frac{16\kappa^2(M-1)^{3/2}}{15\sqrt{2(\gamma+1)}}=0.314\kappa^2(M-1)^{3/2}. \tag{6.15}$$

The value of κ is a constant to be determined by experiments, for example, we have a figure of 0.36 for the turbulent channel flow of incompressible fluid. Although we have no reason to consider the value of κ to be constant in our case, the experimental data most aptly explain it by taking $\kappa=1.7$ as shown in Fig. 6.

These relations can be used as the corrections to the ray-shock theory wherever the similar solution of the perturbed equations (6.7) exists. If the self-similar solution does not exist, that is, if the expression of S (6.11) contains any explicit function of ξ (or η), then an ordinary method such as integration along the each characteristic is necessary in order to solve the equation (6.7). It is not much difficult to obtain the solution for such case but with the present approximate theory the added complexity of such calculations does not seem justified.

7. Experiments

A straight shock tube with constant cross section of 5×20 cm, which has a low pressure chamber 6 m in length and a high pressure chamber 1.5 m in length, was used. A pair of glass windows 8 cm in diameter was attached to the center of the wider side walls 5 m apart from the diaphragm. A pair of contact type shock wave sensers were set 15 cm and 65 cm upstream from the windows. The out-put signals from these sensors were used for the wave speed measurement and for triggering the delay circuit for the spark light source. They are, as shown in Fig. 7, very simple but worked perfectly. Before the run, the low pressure chamber was evacuated and re-filled with dried air to the adjusted pressure. The diaphragm used was of 0.05 mm thick aluminum foil and was broken by a mechanical plunger.

The schlieren photographs and interferograms of the flow field were taken using a spark light souce which is triggered by the delayed signal. The interferometer is a polarization interferometer with the same arrangement as the one reported in

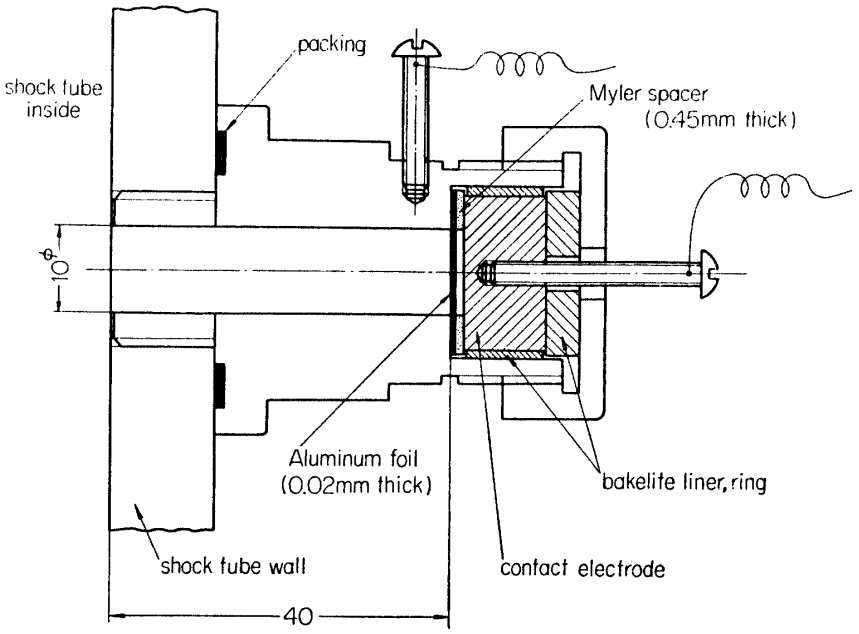

FIGURE 7. The contact type shock wave senser.

the reference [14], which is very easy to construct and can obtain high quality interferograms at a considerably low cost. As shown in the plate, the phase shift obtained by this kind of interferometer corresponds to the density difference between the two points in the flow field apart a distance from each other. Therefore, the interferogram taken by this method shows a double image of the flow field, and the fringe shift at a point in the double image is proportional to the density difference between the two points which happen to make the same image point. Naturally, these interferograms are complicated and not intuitively understandable, but if one of the image points belongs to the undisturbed flow field, then the interferograms show the same character as the ordinary Mach-Zehnder interferometer. All the interferograms were taken at zero fringe condition, then the fringe lines correspond to the isopicnic lines, provided that one of the corresponding image points is in the undisturbed region.

In table 1 the experimental conditions are summarized, including the Reynolds numbers per one centimeter based on the shock wave speed and the gas condition behind the shock in the undisturbed region. The reproducibility of the flow is satisfactory.

TABLE 1 Experimental Conditions

p_0 mmHg	M_1	Re/1 cm
2	2.78	5.4×10^2
4	2.53	1.2×10^3
10	2.20	2.9×10^3
20	1.93	5.8×10^3
40	1.80	1.2×10^4
100	1.51	2.9×10^4

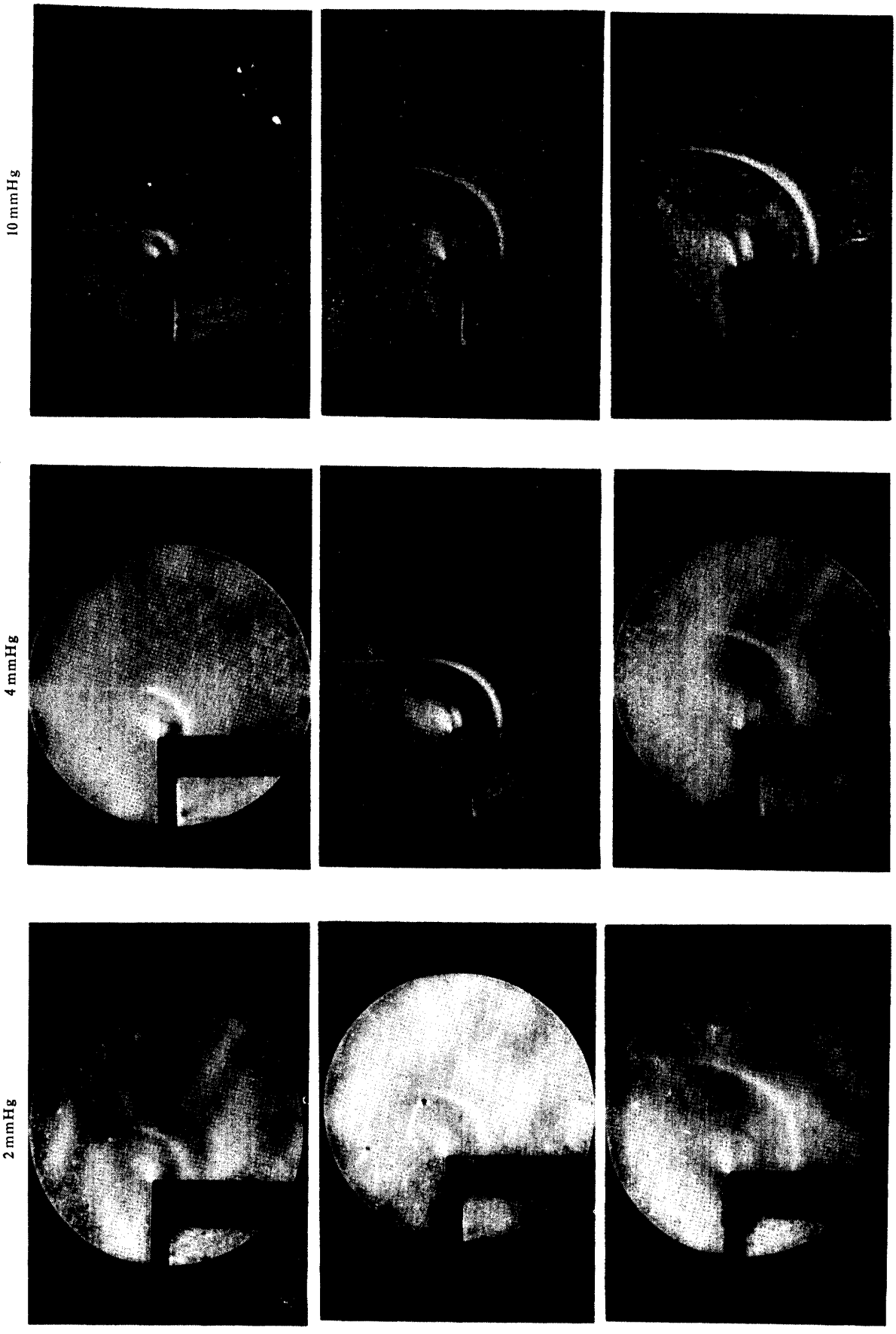

FIGURE 8. Schlieren photographs and interferograms.

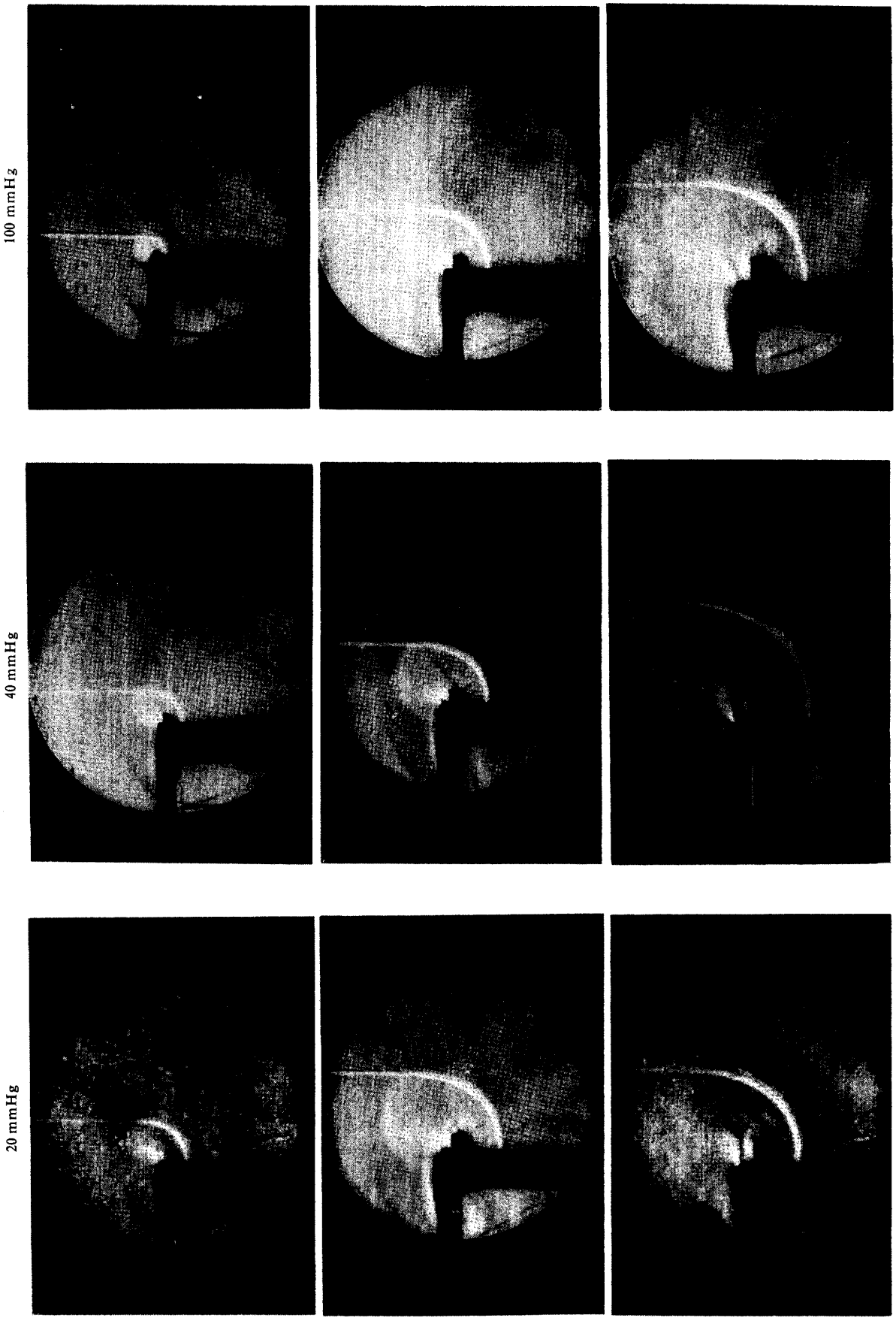

FIGURE 8. Continued.

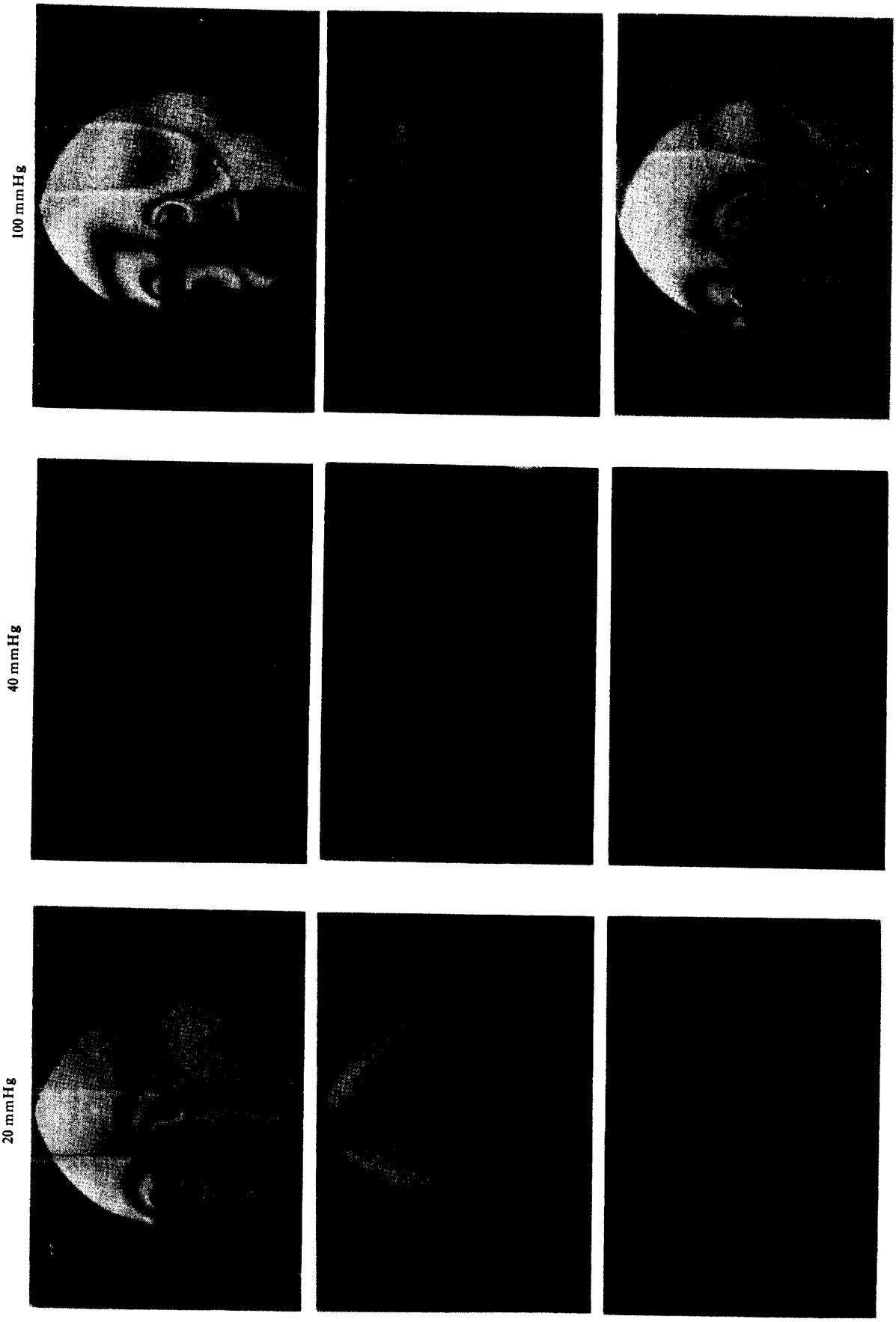

FIGURE 8. Continued.

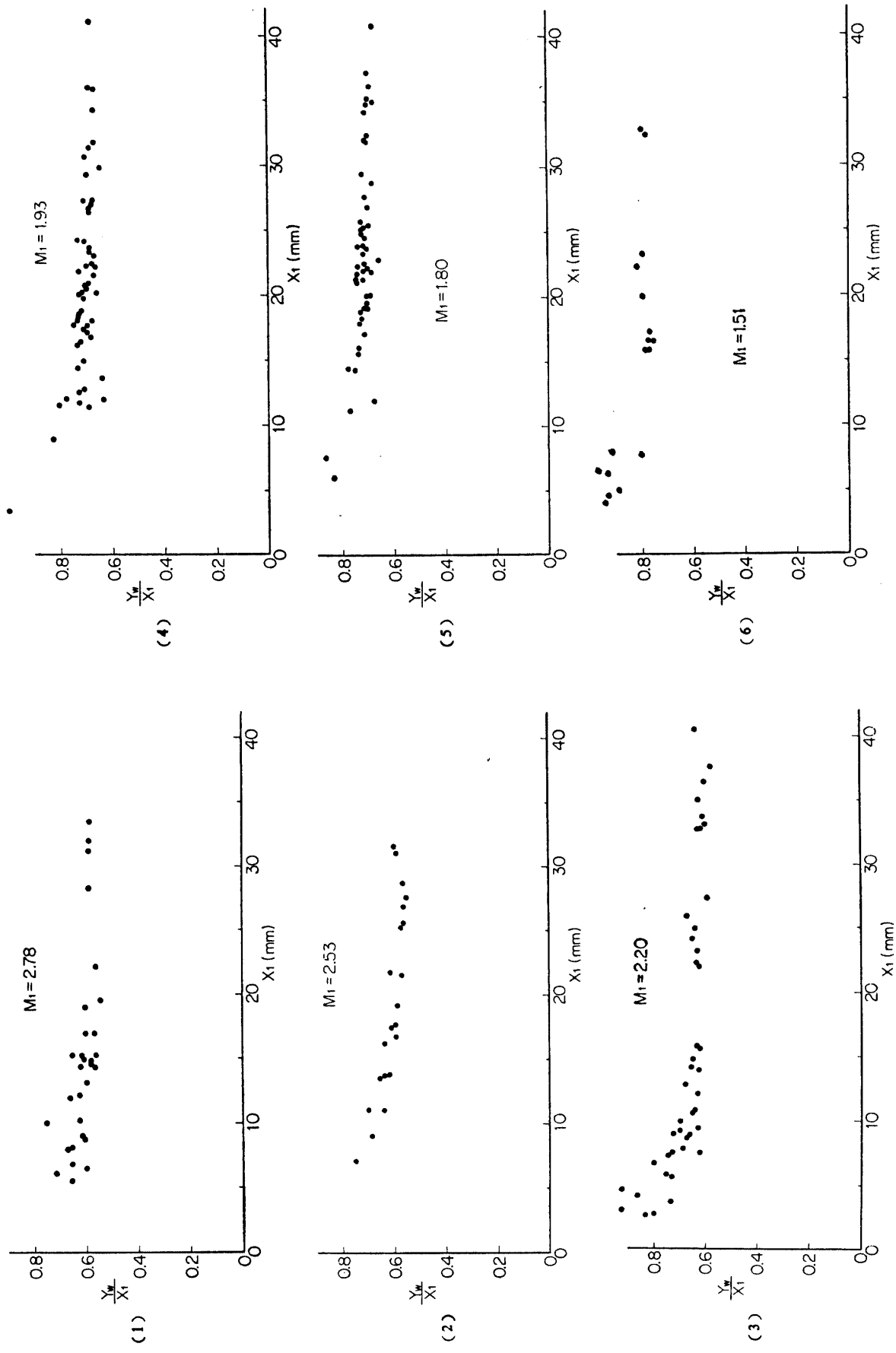

FIGURE 9. Distributions of Y_w/X_1.

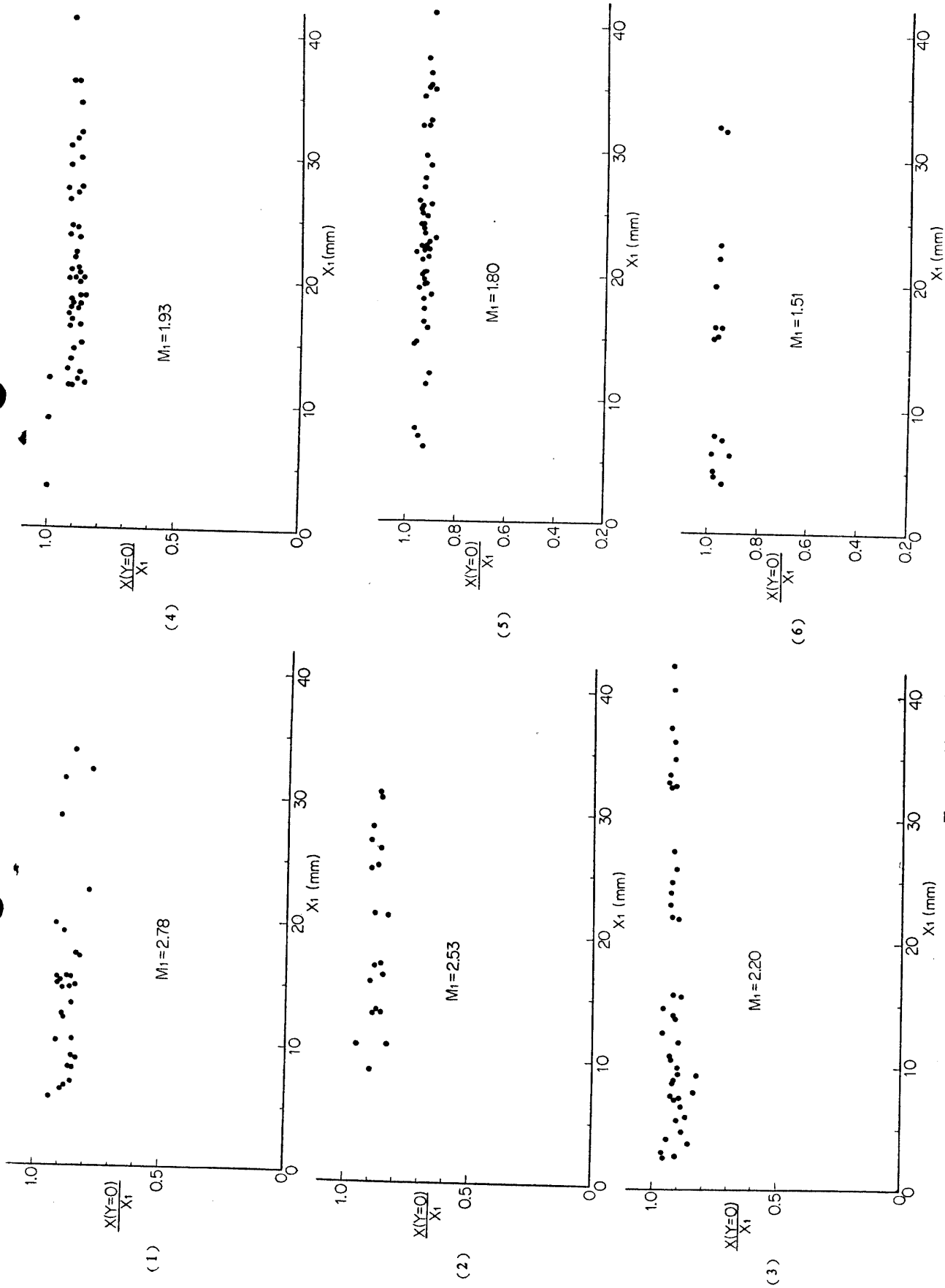

FIGURE 10. Distributions of $X(Y=0)/X_1$.

Fig. 8 shows, as the example, the set of typical shlieren photographs and interferograms. The sensitivity of the optical measurements, it should be kept in mind, is proportional to the undisturbed flow density. The very complicated flow patterns in low Mach number cases may be easily recognized, that is, they show the vortex shedding, the secondary shock, which sometimes is not fully developed yet, and even the flow separation upstream of the corner. The high Mach number cases, on the contrary, show relatively simple patterns.

Fig. 9 shows the ratios of the distances from the corner to the undisturbed shock front (X_1) and those to the diffracted shock wave along the wall (Y_w), being plotted for the former distances. According to the ray-shock theory, they should be constants and correspond directly to the ratio of the Mach numbers of the undisturbed shock wave and those diffracted along the wall. The fact that those points show higher values at the initial stage of the diffraction and take the almost constant value in later period strongly suggests that the mixing process takes place more seriously in the neighbourhood of the corner, where the generalized ray-shock theory, too, naturally cannot be applicable. These constant values at $X_1 \to \infty$ are summarized in Fig. 6, in which the results of the above theories are also presented. There we can easily see the merit of the theories presented in this paper. On the other hand, Fig. 10 shows the distributions of the ratios of $X(Y=0)/X_1$. They indicate no special features in the neighbourhood of the initial part of the diffraction, showing little mixing effect in such region.

The author cannot, admittedly, claim the physically solid bases of this rather arbitrary choice of the mixing mechanism, but it might still be surprising that such simple calculation using the turbulent mixing theory can introduce all the quantitative explanations of the rather complicated shock patterns.

Department of Aerodynamics
Institute of Space and Aeronautical Science
University of Tokyo, Tokyo.
December 25, 1964

References

[1] Forsythe, G.E., Wasow, W.R.: *Finite-difference method for partial differential equations*, Wiley, London (1960)
[2] Pack, D.C., J. Fluid Mech. **18** 549 (1964)
[3] Whitham, G.B., J. Fluid Mech. **2** 145 (1957)
[4] Whitham, G.B., J. Fluid Mech **3** 369 (1959)
[5] Chester, W., Phyl. Mag. (7) **45** 1293 (1954)
[6] Chisnell, R.F., J. Fluid Mech. **2** 286 (1957)
[7] Whitham, G.B., J. Fluid Mech. **4** 337 (1958)
[8] Rościszewski, J., J. Fluid Mech. **8** 337 (1960)
[9] Friedman, M.P., J. Fluid Mech. **8** 193 (1960)
[10] Oshima, K., Aero. Res. Inst. Univ. Tokyo Report 358 (1960)
[11] Whitham, G.B., J. Fluid Mech. **1** 290 (1956)
[12] Friedman, M.P., Kane, E.J., Sigalla, A., AIAA J. **1** 1327 (1963)
[13] Bird, G.A., Wetherall, C.J., AIAA J. **2** 582 (1964)
[14] Françon, M., *Modern applications of physical optics*, New York (1963)
[15] Goldstein, S., *Modern developments in fluid dynamics*, Clarendon Oxford (1938)